**Cite this article**
Archila HF, Rhead A, Ansell MP, Walker P and Lizarazo-Marriaga J (2019)
Elastic response of cross-laminated engineered bamboo panels subjected to in-plane loading.
*Proceedings of the Institution of Civil Engineers – Construction Materials* **172(6)**: 284–295,
https://doi.org/10.1680/jcoma.16.00080

**Research Article**
**Paper 1600080**
Received 05/12/2016;
Accepted 28/03/2017;
Published online 05/05/2017



**Keywords:** materials technology/ strength & testing of materials/ timber structures

**Construction Materials**

ice Publishing

# Elastic response of cross-laminated engineered bamboo panels subjected to in-plane loading

**Hector F. Archila** BArch, PhD, PGDPM
R&D Director, Amphibia BASE Ltd, Bath, UK; Visiting Research Fellow, Department of Architecture and Civil Engineering, University of Bath, Bath, UK (corresponding author: hector.archila@bath.edu)

**Andrew Rhead** MSci(MMath), PhD
Lecturer, Department of Mechanical Engineering, University of Bath, Bath, UK

**Martin P. Ansell** BSc, PhD, FIMMM
Reader, Department of Mechanical Engineering, University of Bath, Bath, UK

**Pete Walker** BSc, PhD, MIEAust, CPEng, CEng, MICE
Director, BRE Centre for Innovative Construction Materials, Department of Architecture and Civil Engineering, University of Bath, Bath, UK

**Juan Lizarazo-Marriaga** MSc, PhD
Associate Professor, Departamento Ingeniería Civil y Agrícola, Grupo de Investigación en Análisis, Diseño y Materiales GIES, Universidad Nacional de Bogotá, Bogotá, Colombia

**Novel cross-laminated bamboo panels comprising three and five layers (G-XLam3 and G-XLam5) were tested in compression along the main (0°) and the transverse (90°) directions. Linear variable differential transformer (LVDT) and non-contact three-dimensional digital image correlation (DIC) measuring techniques were used separately to measure deformation in the elastic region, and the elastic moduli, $Ep_{C,0}$ and $Ep_{C,90}$, were derived. Mean elastic modulus values obtained using LVDTs exhibited a good match with analytically predicted values. In contrast, the elastic values obtained by the DIC method were considerably higher and presented a considerable scatter of results. For instance, the $Ep_{C,0}$ for G-XLam3 and G-XLam5 panels were 17·22 and 15·67 GPa, and 14·86 and 12·48 GPa, using the DIC and LVDT methods, respectively. In general, G-XLam panels with a fifth of the cross-sectional thickness and twice the density of analogous cross-laminated timber exhibited an approximately two-fold increase in $Ep_{C,0}$ and $Ep_{C,90}$. Overall, this research provides guidelines for the assessment and standardisation of the testing procedures for similar engineered bamboo products using contact and non-contact methods and highlights the potential of using G-XLam panels in stiffness-driven applications and in combination with wood for structural purposes.**

## Notation

| | |
|---|---|
| $A$ | cross-sectional area of the panel |
| $Ep_{C,0}$ | compression moduli of elasticity of the panels in the longitudinal direction |
| $Ep_{C,90}$ | compression moduli of elasticity of the panels in the transverse direction |
| $F$ | load |
| $F_{max}$ | maximum permitted load |
| $I$ | moment of inertia to the cross-sectional area (A) |
| $L$ | length |
| $l$ | gauge length (A–B length of the virtual extensometer) |
| $l_0$ | initial length of the extensometer |
| $l_1$ | final length of the extensometer |
| $R_g$ | radius of gyration in two dimensions (2D) |
| $t$ | panel thickness |
| $u$ | deformation |
| $X_1$ | geometric axis corresponding to the longitudinal ($L$) orientation |
| $X_2$ | geometric axis corresponding to the tangential ($T$) orientation |
| $X_3$ | geometric axis corresponding to the radial ($R$) orientation |
| $\Delta L$ | change in length in unit of original length |
| $\varepsilon$ | engineering strain |
| $\lambda$ | slenderness ratio |
| $\rho$ | density |

## 1. Introduction

The bamboo species *Guadua angustifolia* Kunth (Guadua) has been widely used for structural applications in small- and large-scale buildings, bridges and temporary structures in South and Central America (Archila *et al.*, 2012; Hidalgo-López, 2003; Janssen, 2000; Jayanetti and Follett, 1998; Minke, 2012; Trujillo *et al.*, 2013; van der Lugt *et al.*, 2009; Villegas, 2003; Xiao *et al.*, 2008). In addition to its wide availability and low cost, the overall low weight, moderate ductility and high strength of traditional Guadua building systems have been key for its utilisation in this earthquake-prone region (Kaminski *et al.*, 2016). Guadua's high biomass production, renewability and high strength-to-weight ratio make it a potential material for mainstream applications in the construction industry. However, Guadua remains a material for predominantly vernacular construction associated with high levels of manual labour and structural unpredictability (Archila *et al.*, 2012). Additionally, issues regarding poor weathering resistance and incompatibility with conventional building elements diminish its usability in construction.

With the aim of enhancing the use of bamboo in construction, improving its structural predictability and transforming its vernacular image into a more industrialised one, several research projects on hybrid building systems and engineered bamboo products (EBPs) have been implemented (Trujillo and Archila, 2016). Particularly for EBPs using Guadua, Correal *et al.* (2014) characterised the physical and mechanical properties of glue-laminated Guadua (GLG) elements. Their mean values for density and modulus of elasticity (MOE) and ultimate strength in compression parallel to the grain of GLG were 740 kg/m$^3$, 32·27 GPa and 62 MPa, respectively. On the basis of these results, Varela *et al.* (2013) assessed the seismic performance of a wall-sheathing system using wood for the frame and GLG for the walls. Pinilla and Takeuchi-Tam (2012) manufactured solid and sandwich GLG panels, together with T-section beams; while Luna *et al.* (2014a) evaluated the structural connections for a housing project using these GLG panels for wall and beam elements. Making use of modified fibre bundles, Luna and Takeuchi (2014b) manufactured and tested Guadua scrimber beams (a high-density unidirectional material pressed at high temperatures and pressure). They reported mean values for ultimate compressive strength that ranged between 46·6 and 54·08 MPa depending on the adhesive formulation used. Finally, Osorio-Serna *et al.* (2010) extracted technical fibres from Guadua stems and tested their mechanical properties independently and as composites in combination with epoxy resin.

Despite the active research in this field, EBPs from Guadua are scarce and require complex manufacturing processes. For instance, fabrication of GLG products requires an energy-intensive process due to the machining of round culms into rectangular strips that produces high amounts of waste (de Flander and Rovers, 2009; Vogtländer *et al.*, 2010). This process also discards the high-density material at the outside of the stem. On the other hand, extraction of the technical fibres of Guadua also involves complicated mechanical and chemical processes that end up discarding high quantities of the material. Therefore, the development of engineered Guadua products needs to exploit its remarkable features, consider an efficient use of the material through appropriate technology and tackle issues regarding natural variability, irregularity and durability. Research at the University of Bath has devised a manufacturing process using thermo-hydro-mechanical modification (Archila, 2015). These modifications were used as a way of reducing machining and wastage and producing flat Guadua strips (FGS) of controlled thickness and density with improved physical and mechanical properties. Mechanical and physical characterisation of the individual FGS demonstrated an average two-fold increase in density, Young's modulus (Archila *et al.*, 2014) and fibre surface area.

There are significant advantages in cross-laminating these panels to produce products with less mechanical anisotropy and superior surface finish. The results from the individual FGS allowed the prediction of the mean elastic and strength values of cross-laminated Guadua (G-XLam) panels and the simulation of the panel's response to axial compressive load in the longitudinal and transverse directions using finite-element (FE) modelling software (Archila *et al.*, 2014). Validation of these results by mechanical testing of G-XLam3 and G-XLam5 panels was undertaken and its results are presented in this paper. The elastic and mechanical properties of G-XLam3 and G-XLam5 panels were assessed in an axial compression test along (0°) and across their main direction (90°). Physical (contact) and full-field (non-contact) measurement methods were used to track the deformation in the elastic region and the elastic and mechanical properties $Ep_{C,0}$ and $Ep_{C,90}$ of both the panel configurations were evaluated. The digital image correlation (DIC) method was used as the non-contact system to measure strain variations in the $X$, $Y$ (in-plane) and $Z$ axes (out-of-plane) of the panel surface, while linear variable differential transformer (LVDT) transducers were used for the contact system to record deformation along the $X$-axis.

## 2. Materials and methods

Two series of in-plane compression tests of G-XLam3 and G-XLam5 panels were undertaken; one series without and another series with buckling restraints. The first series used the DIC technique to measure deformation and the second used LVDTs. For both test series, the load was kept below the elastic limit and the same panel specimens were used. However, their dimensions varied: the G-XLam3 and G-XLam5 panels for the compression test using DIC were 700 mm × 700 mm, whereas those for the compression tests using LVDTs were 600 mm × 600 mm. The average thickness ($t$) of the G-XLam3 and G-XLam5 panels was 17·5 and 27·5 mm, respectively.

Restraints were required for panel sizes with a slenderness ratio ($\lambda$) over 11 (Bodig and Jayne, 1982), as illustrated in Table 1. For the restrained test series, buckling supports presented an obstacle, which prevented the capture of full-field images of the panel surfaces, thus DIC was not used and deformation was measured using LVDTs. For the unrestrained series, deformation was recorded using the DIC technique and buckling failure was avoided; $\lambda$ was calculated as expressed in the following equation

$$\lambda = \frac{l}{R_g} \quad (1)$$

where $l$ is the length of the column and $R_g$ is the two-dimensional (2D) radius of gyration and is defined as the square root of the ratio of the moment of inertia ($I$) to the cross-sectional area ($A$).

Table 1 compares the slenderness ratio of the G-XLam3 600 × 600 mm and 700 × 700 mm panels. The distribution of

**Table 1.** Slenderness ratio of the G-XLam panels tested

| | G-XLam3 (DIC) (700 × 700 mm) | G-XLam5 (DIC) (700 × 700 mm) | G-XLam3 (LVDT) (600 × 600 mm) | G-XLam5 (LVDT) (600 × 600 mm) |
|---|---|---|---|---|
| $L$: mm | 700 | 700 | 600 | 600 |
| $t$: mm | 16·5 | 27·5 | 16·5 | 27·5 |
| $I$: mm$^4$ | 262 040·25 | 1 213 151·04 | 224 606·25 | 1 039 843·75 |
| $A$: mm$^2$ | 11 550 | 19 550 | 9900 | 16 500 |
| $R_g$: mm | 4·76 | 7·87 | 4·76 | 7·93 |
| $\lambda$ | 147 | 89 | 126 | 75 |

cross-sectional area ($A$) around the G-XLam3 panel's centroid axis or radius of gyration ($R_g$) was almost the same for both panel sizes. Likewise $R_g$ is almost the same for the $600 \times 600$ and $700 \times 700$ mm size G-XLam5 panels.

The panels were tested in the $X_1$ (longitudinal) and $X_2$ (transverse) directions as shown in Figure 1. Two mild steel angle sections were bolted to the top and bottom of the panels to provide vertical alignment and anchorage to the test machine (item 9 in Figure 4). Compression tests of the panels were carried out at a rate of 0·5 mm/min in a hydraulic universal test machine.

The resulting engineering strain ($\varepsilon$) from the compression tests was then calculated as the change in length $\Delta L$ per unit of original length $L$, as expressed in the following equation

$$2. \quad \varepsilon = \frac{\Delta L}{L} = \frac{l_1 - l_0}{l_0}$$

where $l_0$ is the initial length of the extensometer and $l_1$ is its final length.

Load–strain responses from the load cycles of G-XLam3 and G-XLam5 panels were obtained. For both LVDT and DIC testing methods, the normal stress–strain response of each panel was plotted (Figure 2(a)), and a linear regression analysis was performed (Figure 2(b)). The initial part of these graphs that showed the 'parasitic effects' associated with slipping of the test fixture or embedment of the bolts used were discarded for plotting the stress–strain response of the panels.

The mean values for stress and strain obtained from the longest linear portion of the graph between $0{\cdot}1F_{max}$ ($F_1$) and $0{\cdot}4F_{max}$ ($F_2$) were input into Equation 3 to determine the compression MOE of the panels in the longitudinal ($Ep_{C,0}$) and transverse ($Ep_{C,90}$) directions. The maximum permitted load ($F_{max}$) and elastic limit were determined from the preliminary compression test with a control specimen

$$3. \quad Ep_C = \frac{(F_2 - F_1)l}{(u_2 - u_1)A}$$

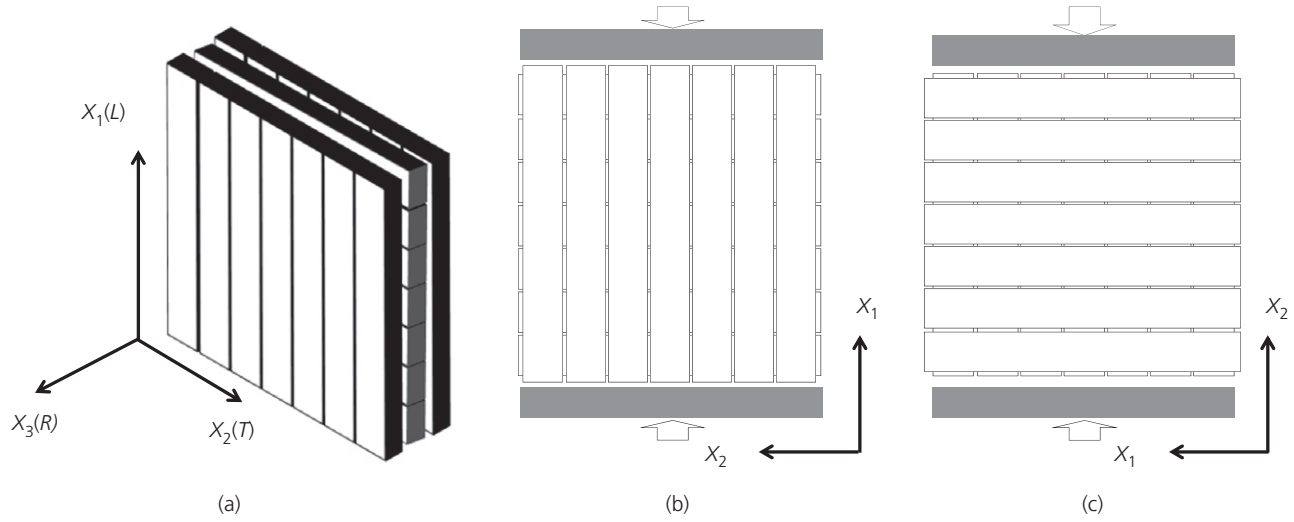


**Figure 1.** (a) Geometric ($X_1$, $X_2$, $X_3$) and orthotropic ($L$, $T$, $R$) axis of the G-XLam panels. (b) Diagram of the compression test in the longitudinal direction of the panel. (c) Diagram of the compression test in the transverse direction of the panel

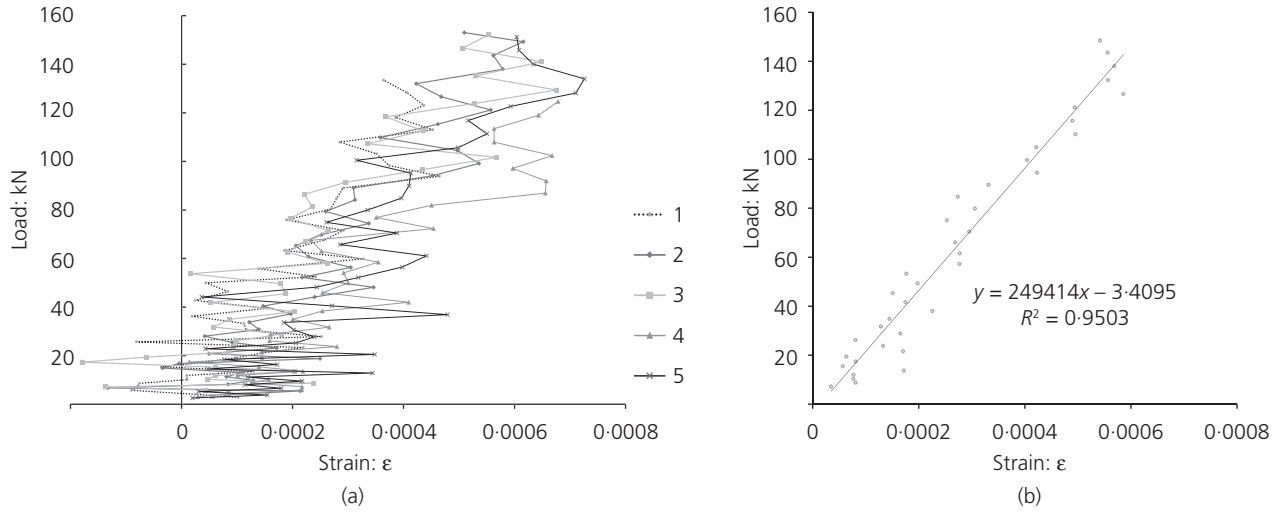


**Figure 2.** (a) Compressive load against compressive strain (DIC) data obtained from in-plane compression tests on the G-XLam5 panel tested along the longitudinal, $X_1$ axis and (b) average load against strain graph derived from the DIC data

where $F_2 - F_1$ is the increment of load between $0{\cdot}1F_{max}$ and $0{\cdot}4F_{max}$; $u_2 - u_1$ is the increment of deformation corresponding to $F_2 - F_1$; $l$ is the gauge length (A–B length of the virtual extensometer); and $A$ is the cross-sectional area of the panel.

## 3. Compression test using DIC

DIC was used to produce an overall picture of deformation of G-XLam3 and G-XLam5 panels and carry out strain measurements on their surface when subjected to in-plane compression load. Two monochrome high-speed cameras (Fast Cam SA3, items 2 and 3 in Figure 3) fitted with Nikon 24–85 mm lenses (AF-D Nikkor f/2·8–4) recorded simultaneous images of the speckle pattern painted on the surface of the G-XLam panel (item 1 in Figure 4) at a rate of one frame per second. Both cameras were mounted on a tripod rail that was parallel to the panel and positioned at a stereo angle below 60° (item 7 in Figure 3). Adjustable light-emitting diode ring lamps fixed to the lenses provided additional illumination (item 11 in Figure 3). Sharp focus, adequate illumination and correct brightness were controlled on screen with the aid of the recording software Photron Fastcam. A monitor displaying the load and stroke readings (item 4 in Figure 3) from the test machine was positioned in the field of view of one of the cameras.

Prior to testing, a calibration grid with 12 mm dots spaced at 34·93 mm intervals (item 10 in Figure 3), which covered the full field of view, was gently moved in front of the panel, and sets of ~60 images were recorded. Rotation about all three axes permitted the calibration of the stereo-vision system. These images were then analysed using the calibration tool of the VIC-3D 2009 software and a low overall error (standard deviation of residuals) for all views ($e \leq 0{\cdot}015$ – given by the software (Correlated Solutions, 2010)) was ensured before running the test. Both recording and analysing software were installed on a laptop with sufficient processing and storage capacity. A reference image was taken once the calibration was performed and before the application of load.

The panels were loaded five times below the elastic limit so that buckling failure was avoided. During testing, the master and slave cameras captured consecutive images of the full field of view, and the increase in load and the corresponding deformations in the $X$, $Y$ (in-plane) and $Z$ (out-of-plane) axes of the panel were viewed from a monitor (item 7 in Figure 4) placed to one side.

It was then possible to track both load and strain for each pair of captured images. These sets of paired images were analysed using VIC-3D 2009 software, and 2D and three-dimensional (3D) strain maps (Figure 5) of the pre-defined area of interest (area of interest, item 8 in Figure 4) were produced. Regions with spikes or noise were avoided and a subset value of 21 (size of the tracking grid of points) and step size of five pixels (distance between the points tracked by the software) was chosen for the DIC analysis. The resulting strain in $X$, $Y$ and $Z$ axes was calculated using the VIC-3D 2009 software.

Using VIC-3D 2009 software, a virtual extensometer (A–B) was placed at the mid-point and mid-height of the reference

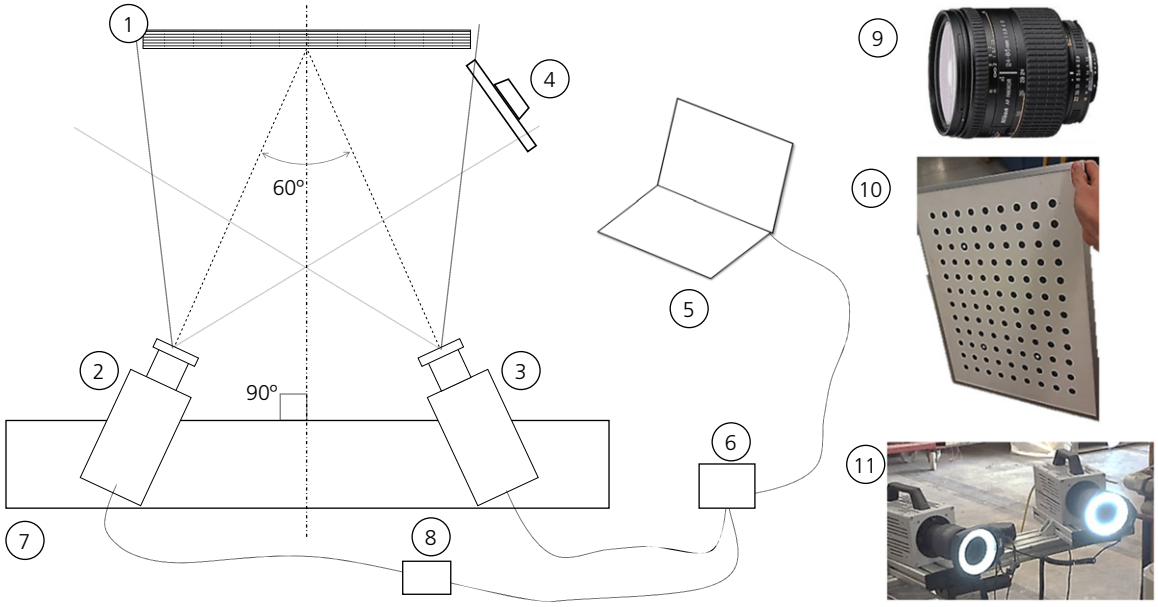


1. Object: G-XLam panel
2. Master camera
3. Slave camera
4. Load display: Monitor
5. Laptop
6. Router
7. Tripod rail
8. Remote shutter switch
9. Nikon lenses 24–85 mm
10. Calibration grid
11. LED lighting

**Figure 3.** DIC test configuration and instrumentation

image of each G-XLam panel (Figures 5(a) and 5(b)), and the axial strain variation for all the captured images was calculated. Typical stress–strain responses were plotted for both panels and orientations, and a linear regression analysis was performed for each configuration.

## 4. Compression test using LVDT

An in-plane compression test using LVDTs and buckling restraints was undertaken on the G-XLam3 and G-XLam5 panels and the results were compared with those obtained using the DIC technique. A compressive load was applied to the two G-XLam (one G-XLam3 and one G-XLam5) panels with a 2000 kN Dartec universal testing machine (Figure 6) at a rate of 0·5 mm/min.

Each panel was tested in the longitudinal ($X_1$) and transverse ($X_2$) directions (Figures 6(b) and 6(c)) and was fixed to the testing machine using the fixture shown in Figure 6(a) (item 2). Buckling restraints with Teflon attached to the specimen and wooden blocks were placed vertically (item 3 in Figure 6) and deformation at 0°, 45° and −45° to the load application axis was measured by LVDTs (items A, B, C and D in Figure 6). LVDTs A, B and C measured displacement variations from zero to 25 mm, while LVDT D had a maximum range of 100 mm. Deformation was recorded by a Vishay 5000 data logger. Data from seven load cycles for each panel configuration and test direction were collated and load–deformation was plotted following the same procedure as with the DIC testing method. A linear regression analysis was performed for each load cycle and the straight part of these graphs between $0{\cdot}1F_{max}$ and $0{\cdot}4F_{max}$ (elastic region) were input into Equation 3 to determine the longitudinal ($L$) and transverse ($T$) MOE ($L = Ep_{C,0}$ and $T = Ep_{C,90}$) of the G-XLam3 and G-XLam5 panels.

## 5. Results and discussion

### 5.1 Determination of $E_0$ and $E_{90}$ of G-XLam panels by compression test using DIC

Engineering strain values obtained from the virtual extensometer placed (A–B) on G-XLam3 and G-XLam5 panels were used for the calculation of MOE in compression in both transverse ($X_2$) and longitudinal ($X_1$) orientations ($E_0$ and $E_{90}$, respectively).

$Ep_{C,0}$ and $Ep_{C,90}$ results for G-XLam3 and G-XLam5 are presented in Table 2. As can be observed in this table, the mean MOE values for both panels in the transverse direction ($Ep_{C,90}$) are considerably lower and present high coefficients of variation (CoV). This can be attributed to the significant

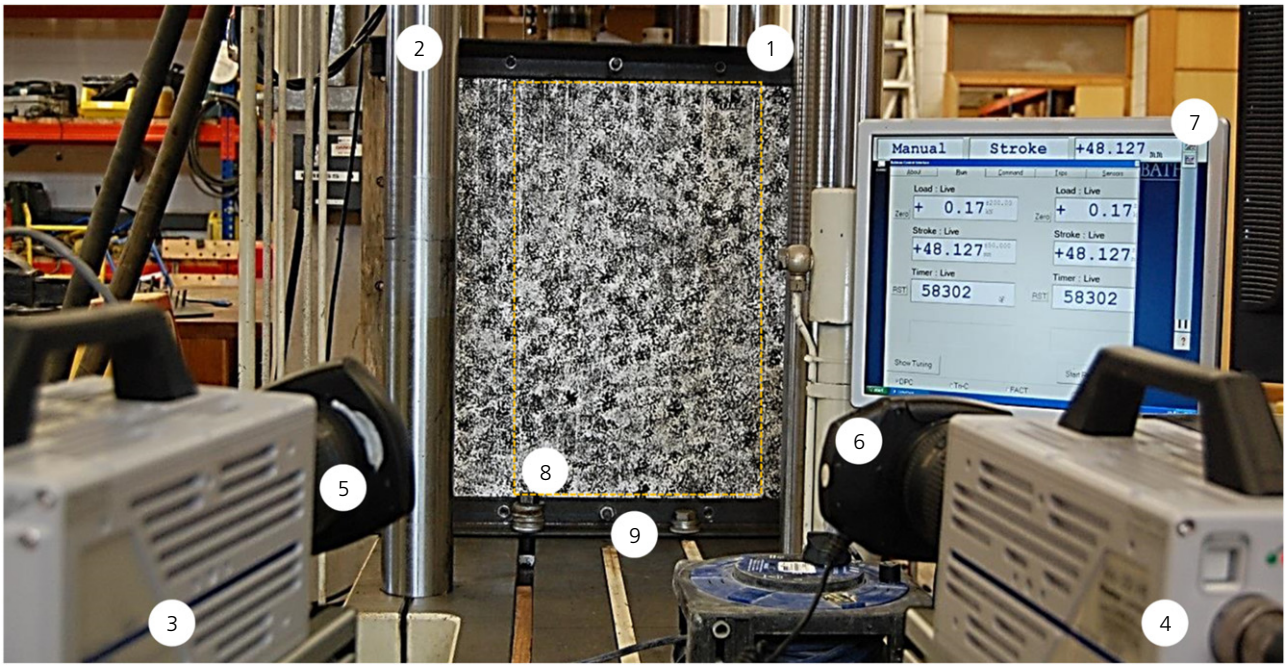


1. Object: G-XLam panel
2. Mayes 20 kN test machine
3. Master camera
4. Slave camera
5. Nikon lenses 24–85 mm
6. LED lighting
7. Load display: monitor
8. Area of interest
9. Angle sections

**Figure 4.** Set-up for the compression test of CLG panels using the DIC method

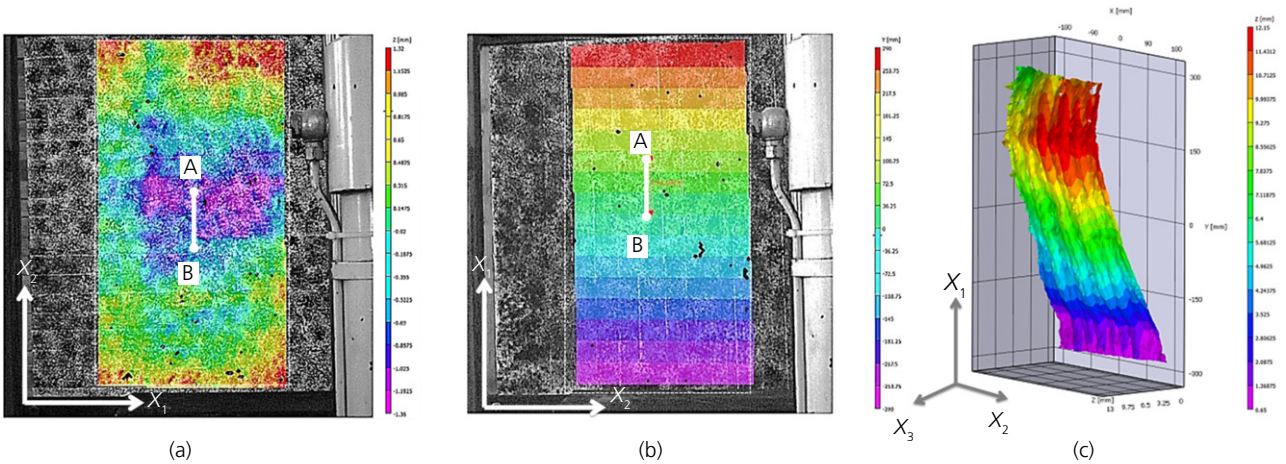


(a) (b) (c)

**Figure 5.** (a) Strain map in $X_3$ (radial) direction of a G-XLam panel tested in compression along $X_2$ (transverse) axis, (b) strain map resulting in $X_1$ of a G-XLam panel tested in compression along $X_1$ (longitudinal) axis and (c) axonometric view of the 3D strain map of the deformation in $z$ ($X_3$) of the CLG-3 panel tested in compression $E_0$ (scale on the 3D strain map is exaggerated)

slenderness ratio ($\lambda$) of the panels that caused rapid out-of-plane deformation (buckling) and forced the test to be stopped at low load levels. As a result, strain results from the DIC analysis experienced high scatter. The effect of buckling was critical for the G-XLam3 panels tested in the transverse direction ($X_2$), which resulted in an extremely low value of $Ep_{C,90}$

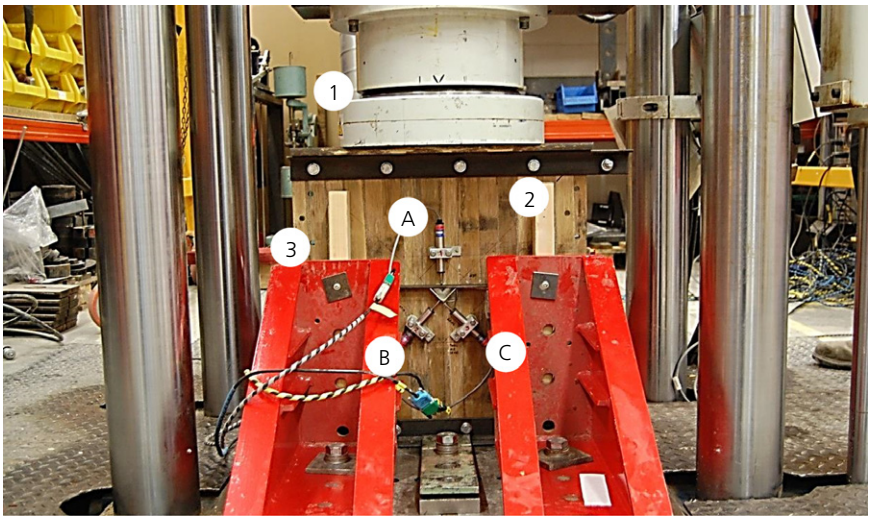


(a)

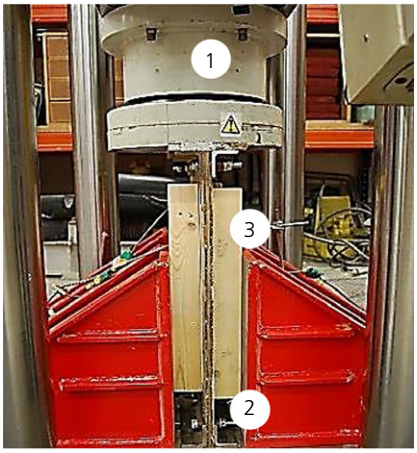


(b)

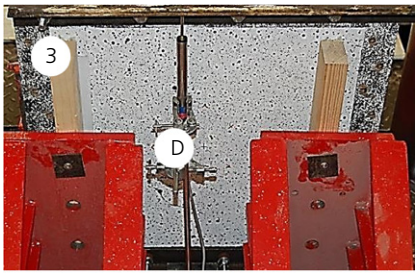


(c)

1. Test machine crosshead
2. LL-double steel angle section
3. Buckling restraint-timber blocks
A. 0–25 mm range LVDT at 0°
B. 0–25 mm range LVDT at 45°
C. 0–25 mm range LVDT at –45°
D. 0–100 mm range LVDT at 0°

**Figure 6.** In-plane compression test set-up using LVDT and buckling restraints: (a) frontal view, (b) lateral view and (c) back face of the panel under test

(mean = 2·43 GPa). Although the $Ep_{C,90}$ results for the G-XLam5 panels presented a considerably higher dispersion of values around the mean (CoV ~ 44%), the buckling effect was minor due to the reduced slenderness ratio, $\lambda = 89$ for G-XLam3, while for G-XLam5 it was $\lambda = 147$.

Out-of-plane deformation was recorded by the stereovision cameras and analysed using the DIC method producing 3D strain maps for each panel configuration (Figure 7). Manufacturing imperfections were observed using the DIC; however, these surface defects did not exceed ±2 mm in-plane (measured linearly on the $Z$-axis). The maximum in-plane compression load applied to the G-XLam3 and G-XLam5 panels along the longitudinal direction ($X_1$) was seven and four times the load applied transversely, respectively. This allowed small out-of-plane deflections without failure.

The strain results from one of the G-XLam3 panel specimens tested in in-plane compression, which failed in buckling, were discarded for the calculation of the MOE. Figure 8 illustrates this failure and indicates the presence of gaps that triggered the failure.

### 5.2 Determination of $E_0$ and $E_{90}$ of G-XLam panels by compression test using LVDT

Global compressive deformation of the G-XLam panels recorded from LVDT-D was used for calculating strain and

**Table 2.** MOE results for G-XLam panels using DIC

| $Ep_{C,0,90} = \frac{(F_2 - F_1)l}{(u_2 - u_1)A}$ | G-XLam3 | | G-XLam5 | |
|---|---|---|---|---|
| | $Ep_{C,0}$: GPa | $Ep_{C,90}$: GPa | $Ep_{C,0}$: GPa | $Ep_{C,90}$: GPa |
| Cycle 1 | 18·65 | 2·92 | 18·53 | — |
| Cycle 2 | 15·25 | 3·18 | 11·42 | 10·87 |
| Cycle 3 | 14·20 | 1·86 | 14·34 | 7·24 |
| Cycle 4 | 15·84 | 1·64 | 18·56 | 5·14 |
| Cycle 5 | 22·16 | 2·43 | 15·67 | 14·59 |
| Mean | 17·22 | 2·43 | 15·67 | 9·46 |
| SD | 3·22 | 0·66 | 3·02 | 4·16 |
| CoV | 19% | 27% | 19% | 44% |

Equation 3 for the calculation of the $Ep_{C,0}$ and $Ep_{C,90}$; the results are presented in Table 3.

The deformation recorded from the LVDT A positioned at the centre mid-height point of the panels was not representative for calculating the axial strain of the panel during the compression test. The recorded mean values from LVDTs A, B and C were neglected, as values obtained for deformation ($\delta$) fluctuated between 1 and 10 μm (0·01 mm > $\delta \leq$ 0·001 mm = 1 μm), which were below the precision range of the LVDTs (±0·025 mm for the 25 mm and ±0·2 mm for the 100 mm range LVDT) and resulted in extremely small strains and hence very large MOE values. This was due to the reduced area in which the axial deformation was recorded that did not experience significant deformation (as observed during compression test using DIC) and the increased stiffness of the panel resulting from the use of buckling restraints. During data analysis, misalignment and embedment effects were accounted for and the linear elastic region of the test was used for the calculation of $Ep_{C,0}$ and $Ep_{C,90}$.

Results from in-plane compression tests of G-XLam3 and G-XLam5 panels using DIC and LVDT are presented in Table 4 together with the predicted and FE values reported in Archila *et al*. (2014). These values have been updated for the conditions of the tests described in this paper. $Ep_{C,0}$ and $Ep_{C,90}$ depend on the number of layers and the stiffness of the individual layers (i.e. $E_L$ and $E_T$ in Archila *et al*. (2014)).

Independently of the method used (DIC, LVDT or analytical), the mean values of the elastic properties in longitudinal compression ($Ep_{C,0}$) are about 50 and 70% higher than the mean elastic properties measured in the transverse direction ($Ep_{C,90}$) for G-XLam3 and G-XLam5 panels, respectively. In spite of the considerably low mean value for $Ep_{C,90}$ obtained from the DIC test of G-XLam3 panels, in general the DIC values were higher than the analytical predictions and test results using LVDT. This can be attributed to the significant slenderness ratio ($\lambda$) of the G-XLam3 panels that caused rapid out-of-plane deformation (buckling) and forced the test to be stopped at low load levels (no restraints were used on DIC specimens). As a result, the strain values from the DIC analysis experienced high scatter. The effect of buckling was critical for the G-XLam3 panels tested in the transverse direction, which resulted in an extremely low value of $Ep_{C,90}$ (2·43 GPa). Although, $Ep_{C,90}$ results for the G-XLam5 panels presented a considerably higher dispersion of values around the mean (CoV ~ 44%), the buckling effect was minor due to the reduced slenderness ratio – that is, $\lambda = 89$ for G-XLam3 and $\lambda = 147$ for G-XLam5. Additionally, the test with DIC resulted in high variability of results; CoV for the compression test, values reached up to 44%. The analytical values provided a reasonably accurate prediction of the elastic properties of the G-XLam3 and G-XLam5 panels. Variability of the predicted compressive modulus ($Ep_{C,0}$ and $Ep_{C,90}$) of both panel configurations was below 7%, when compared with the mean test results using physical measurement systems (LVDT). No permanent deformation (post-test) in any axis was recorded by the DIC; however, the 3D strain maps showed areas prone to deformation in the $X_3$ ($R$) direction that presented gaps or fabrication defects.

Overall, an adequate match between the predictions and the test results using physical (contact) measurement techniques was found for assessing the elastic properties of the panels. In contrast, the mean elastic values obtained by the DIC method were considerably higher and presented a considerable scatter of results (CoV). Although this was not the case for all the images, this can be improved in future tests by selecting a larger subset. This can reduce the variation and 'noise' seen in some pictures (black holes); nevertheless, the ultimate results will be similar to the obtained values. Differences among the results were most likely caused by manufacturing flaws and thickness variation within the individual lamellas, as seen in Figure 9; unfortunately, their influence could not be statistically determined due to the use of only one test specimen per panel configuration (G-XLam3 and G-XLam5). However, simulations undertaken through FE analysis showed that

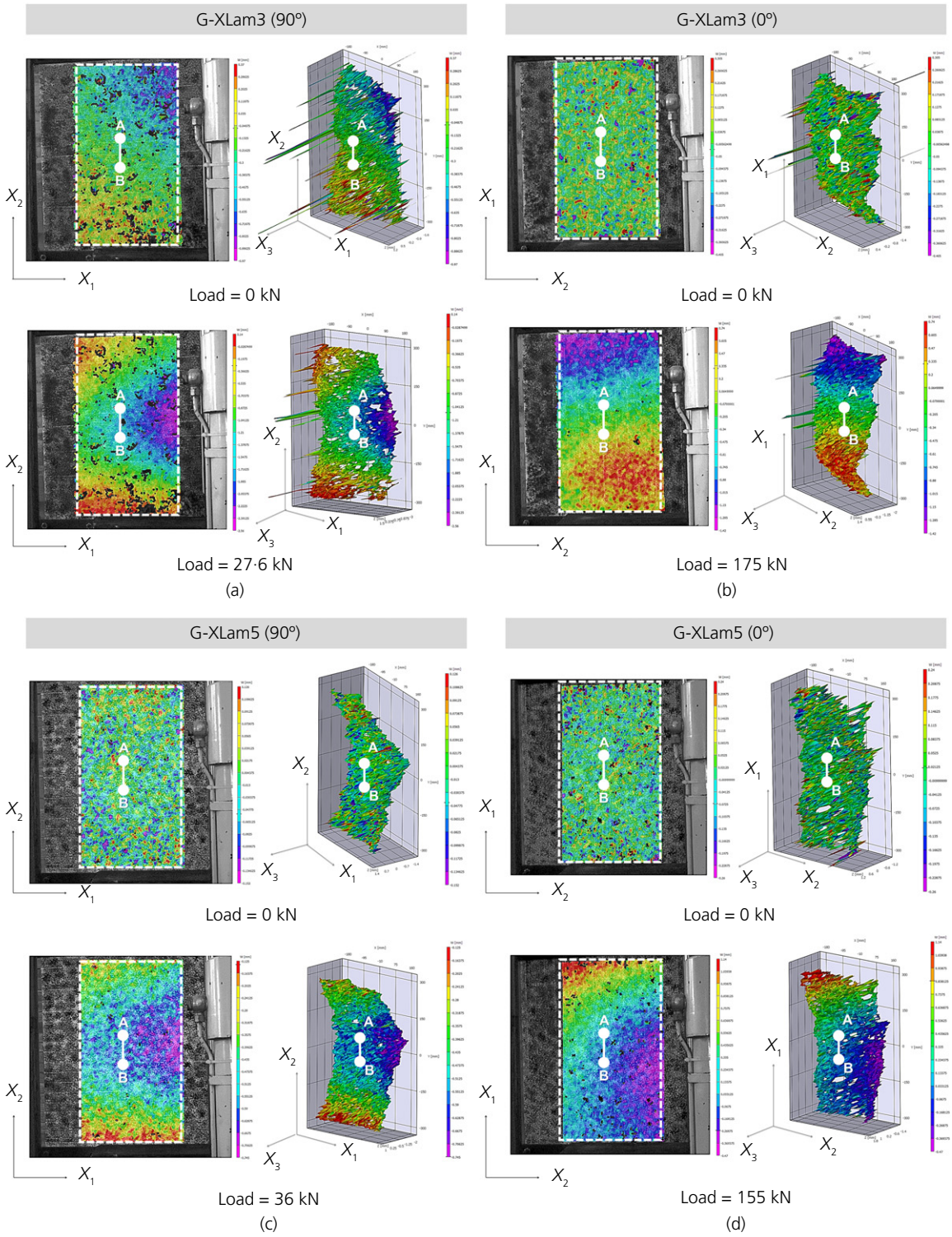


**Figure 7.** Front views and axonometric projections of the 3D strain maps produced using DIC method during in-plane compression test for G-XLam3 and G-XLam5 panels: (a) G-XLam3 panel tested along the transverse ($X_2$) direction, (b) G-XLam3 panel tested along the longitudinal ($X_1$) direction, (c) G-XLam5 panel tested along the transverse ($X_2$) direction and (d) G-XLam5 panel tested along the longitudinal ($X_1$) direction

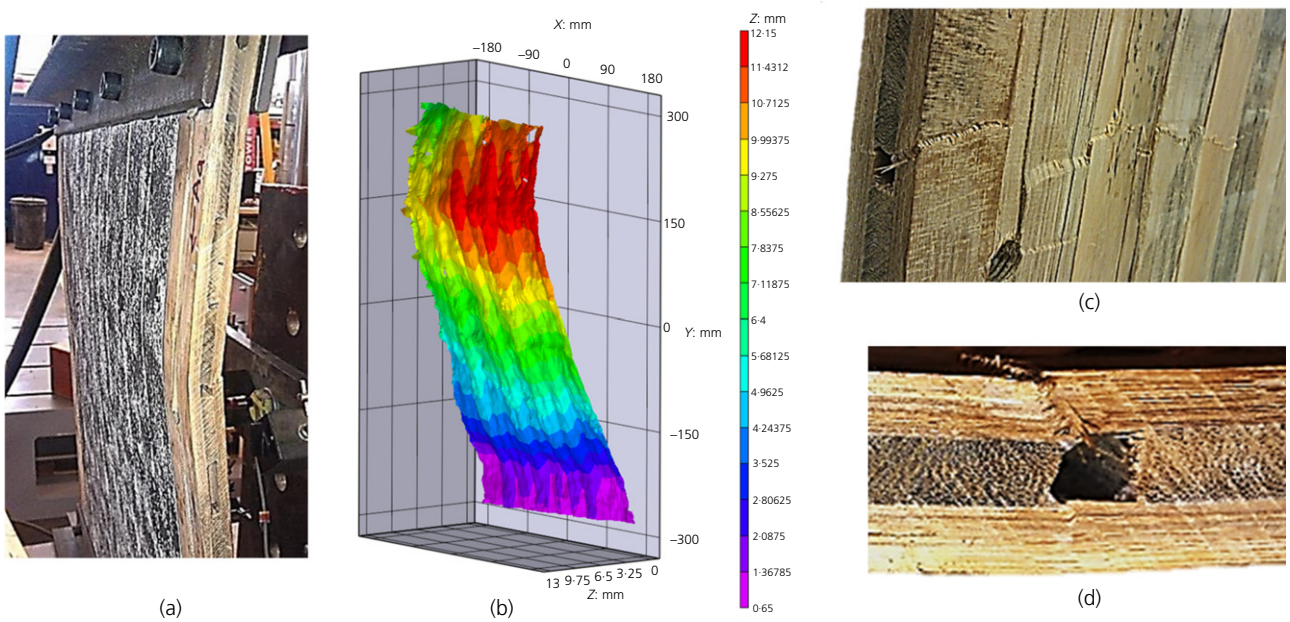


**Figure 8.** G-XLam3 panel discarded for buckling failure during compression test using DIC: (a) failure of panel mounted on the test machine, (b) 3D-strain map of the failure, (c) detail of the failure area and (d) detail of the shear failure produced by the buckling effect during compression test

**Table 3.** Elastic mechanical properties of G-XLam panels obtained from compression test using LVDTs

| **Specimen** | **G-XLam3 (*L*)** | **G-XLam3 (*T*)** | **G-XLam5 (*L*)** | **G-XLam5 (*T*)** |
|---|---|---|---|---|
| Property | $Ep_{C,0}$: GPa | $Ep_{C,90}$: GPa | $Ep_{C,0}$: GPa | $Ep_{C,90}$: GPa |
| Mean | 14·86 | 7·43 | 12·48 | 8·74 |
| SD | 1·17 | 0·69 | 0·92 | 0·76 |
| CoV | 8% | 7% | 7% | 9% |

**Table 4.** Summary of the results obtained from the in-plane compression panel testing and the FE and predicted values previously obtained by Archila *et al*. (2014)

| | **G-XLam3 ($t$ = 17·5 mm; $\rho$ = 890 kg/m$^3$)** | | **G-XLam5 ($t$ = 27·5 mm; $\rho$ = 890 kg/m$^3$)** | |
|---|---|---|---|---|
| | $Ep_{C,0}$: GPa | $Ep_{C,90}$: GPa | $Ep_{C,0}$: GPa | $Ep_{C,90}$: GPa |
| DIC test | 17·22 | 2·43 | 15·67 | 9·46 |
| SD | 3·22 | 0·66 | 3·02 | 4·16 |
| CoV | 19% | 27% | 19% | 44% |
| LVDT test | 14·86 | 7·43 | 12·48 | 8·74 |
| SD | 1·17 | 0·69 | 0·92 | 0·76 |
| CoV | 8% | 7% | 7% | 9% |
| Predicted | 14·83 | 7·93 | 13·45 | 9·31 |
| FE model (gapless) | 20·69 | 10·75 | 18·70 | 12·66 |
| FE model (with gaps) | 18·75 | 9·56 | 16·94 | 11·42 |
| CLT M1 BSP crossplan (predicted)[a] | CLT 3 ($t$ = 78 mm; $\rho \sim$ 480 kg/m$^3$) | | CLT 5 ($t$ = 134 mm; $\rho \sim$ 480 kg/m$^3$) | |
| | 7·57 | 3·91 | 6·74 | 4·62 |

[a] Values predicted using mean values of spruce (*Picea abies*) C24 used in M1 BSP crossplan CLT panels (Mayr-Melnhof Kaufmann Group, 2009)

**Figure 9.** Thickness variation and gaps across the section of a G-XLam5 panel

manufacturing defects such as the gaps between lamellas in the faces of the panel had a direct effect on the elastic properties predicted (Table 4).

## 6. Conclusions

The mechanical properties of the G-XLam panels were calculated using mean elastic values obtained from previous tests of small clear specimens, subsequently characterised through mechanical testing using the DIC method and finally validated with a FE model. The mean elastic values from DIC for the G-XLam3 and G-XLam5 panels were 17·22 and 15·67 GPa in the main direction ($Ep_{C,0}$) and 2·43 and 9·46 GPa in the transverse direction ($Ep_{C,90}$), while the mean elastic values from LVDTs for the G-XLam3 and G-XLam5 panels were 14·86 and 12·48 GPa in the main direction ($Ep_{C,0}$) and 7·43 and 8·74 GPa in the transverse direction ($Ep_{C,90}$). As expected, the higher stiffness of the G-XLam3 panels along the main direction is due to the proportionally higher ratio of material longitudinally orientated along the loading direction (i.e. 0·66 in G-XLam3 and 0·6 in G-XLam5 panels). Similar mean MOE values from mechanical testing in longitudinal compression ($Ep_0 = 14$ GPa) have been reported by Verma and Chariar (2012) for five-layer cross-laminated bamboo products using different manufacturing and testing techniques. This research has pioneered the use of DIC techniques for the measurement of deformation on EBPs. However, mean values obtained using this method were higher and presented a higher variability than the analytical predictions and test results using LVDTs. Although there is great potential for the use of this type of non-contact measurement methods for remote and non-destructive testing of materials and structures, further testing and improvements to the DIC method in bio-based materials such as EBPs are required. For instance, adjustments on the speckle pattern and the subset size (e.g. a larger subset) might result in a lower CoV.

Furthermore, the mean results for the mechanical properties of G-XLam panels obtained in this research are higher than the characteristic elastic values of comparable engineered wood products (e.g. cross-laminated timber (CLT) panels). A comparison of the LVDT and predicted results for G-XLam panels with those of analogous CLT panels (M1 BSP crossplan by Mayr-Melnhof Holz) shows an approximately two-fold increase in density and MOE (Table 4). That is, the in-plane compression MOEs of these CLT panels in the main direction ($Ep_{C,0}$) and transverse direction ($Ep_{C,90}$) were about half of that of G-XLam panels (e.g. $Ep_{C,0}$ was 7·57 GPa and 14·83 GPa for CLT3 and G-XLam3 panels, respectively). On the other hand, the thickness of G-XLam3 and G-XLam5 panels is almost one-fifth of CLT3 and CLT5 panels (e.g. thicknesses of CLT5 and G-XLam5 were 134 and 27·5 mm, respectively). This is a desirable feature in stiffness-driven design, but the high slenderness of G-XLam elements presents a structural challenge in overcoming buckling. For instance, potential engineering applications for G-XLam panels are sandwich panels and stressed skin structures (e.g. monocoque), where thin but very stiff layers are separated by a core or internal structure that increases the second moment of area and reduces buckling. This highlights the potential of EBPs such as G-XLam, as a complementary material (not a substitute) in structural applications combined with wood and/or lightweight cores to provide the required stiffness with a reduced cross-section. However, further testing, research and understanding of the mechanical behaviour of EBPs is required, together with the optimisation of current manufacturing processes and their incorporation within timber standards for structural design. Although there are no standards for EBPs, this research has made use of the timber engineering knowledge and standardised methods for engineered wood products, which makes timber standards a feasible framework for the assessment of EBPs.

## Acknowledgements

The authors are grateful to Amphibia Group SAS (Colombia), Amphibia BASE Ltd (UK) and COLCIENCIAS, for the financial support provided, and to Grupo de Investigación en Análisis, Diseño y Materiales (GIES) at Universidad Nacional de Colombia (Bogotá) for the materials provided and logistical support given during the execution of the research.

**REFERENCES**

Archila HF (2015) *Thermo-Hydro-Mechanically Modified Cross-Laminated Guadua-Bamboo Panels*. PhD thesis, University of Bath, Bath, UK.

Archila HF, Ansell MP and Walker P (2012) Low carbon construction using Guadua bamboo in Colombia. *Key Engineering Materials* **517**: 127–134, http://dx.doi.org/10.4028/www.scientific.net/KEM.517.127.

Archila HF, Brandon D, Ansell MP, Walker P and Ormondroyd GA (2014) Evaluation of the mechanical properties of cross laminated bamboo panels by digital image correlation and finite element modelling. In *Proceedings of the World Conference on Timber Engineering, Quebec, QC, Canada* (Salenikovich AJ (ed.)). WCTE 2014, Quebec, QC, Canada, p. 43.

Bodig J and Jayne BA (1982) *Mechanics of Wood and Wood Composites*, Reprint ed. Van Nostrand Reinhold Company, New York, NY, USA.

Correal J, Echeverry J, Ramírez F and Yamín L (2014) Experimental evaluation of physical and mechanical properties of glued laminated *Guadua angustifolia* Kunth. *Construction and Building Materials* **73**: 105–112, http://dx.doi.org/10.1016/ j.conbuildmat.2014.09.056.

Correlated Solutions (2010) *Vic-3D 2010, Testing Guide*. Correlated Solutions Inc., Irmo, SC, USA.

de Flander K and Rovers R (2009) One laminated bamboo-frame house per hectare per year. *Construction and Building Materials* **23(1)**: 210–218.

Hidalgo-López O (2003) *Bamboo: The Gift of the Gods*, 1st edn. D'vinni Ltda, Bogotá, DC, Colombia.

Janssen JJA (2000) *Designing and Building with Bamboo*. Kumar, ed. INBAR-International Network for Bamboo and Rattan, Eindhoven, the Netherlands, INBAR Technical Report No. 20A.

Jayanetti DL and Follett PR (1998) *Bamboo in Construction, an Introduction*. TRADA Technology, Ltd, Buckinghamshire, UK, INBAR Technical Report No. 15.

Kaminski S, Lawrence A and Trujillo D (2016) *Design Guide for Engineered Bahareque Housing*. INBAR – International Network for Bamboo and Rattan, Beijing, China.

Luna P, Olarte AM and Takeuchi-Tam CP (2014a) Análisis teórico experimental de conexiones en elementos estructurales de bambú guadua laminado pegado prensado, para un proyecto de vivienda. *Dyna Journal of the Facultad de Minas, Universidad Nacional de Colombia-Sede Medellín* **81(184)**: 110–114 (in Spanish).

Luna P and Takeuchi-Tam CP (2014b) Resistencia mecánica de elementos de fibra de Guadua compactada. In *Proceedings of the II Simposio Internacional Guadua y Bambú* (Díaz-Ariza LA (ed.)). Editorial Pontificia Universidad Javeriana, Bogotá, DC, Colombia, p. 119–125 (in Spanish).

Minke G (2012) *Building with Bamboo: Design and Technology of a Sustainable Architecture*. Walter de Gruyter, Basel, Switzerland.

Mayr-Melnhof Kaufmann Group (2009) *Manual Cross-Laminated Timber Panels M1 BSP Cross Plan*. M-MKG, Gaishorn am See, Austria.

Osorio LR, Trujillo De Los Ríos EE, van Vuure AW *et al.* (2010) The relation between bamboo fibre microstructure and mechanical properties. *Proceedings of the 14th European Conference on Composite Materials, Budapest, Hungary*, p. 10.

Pinilla JJ and Takeuchi-Tam CP (2012) The structural behaviour of laminated-Guadua panels under parallel plane loads. *Ingeniería e Investigación* **32(2)**: 18–22.

Trujillo D and Archila HF (2016) *Engineered Bamboo and Bamboo Engineering*. Exova BM TRADA, Buckinghamshire, UK.

Trujillo DJA, Ramage M and Chang WS (2013) Lightly modified bamboo for structural applications. *Construction Materials* **166(CM4)**: 238–247, http://dx.doi.org/10.1680/coma.12.00038.

van der Lugt P, Vogtländer J and Brezet H (2009) *Bamboo, a Sustainable Solution for Western Euope Design Cases, LCAs and Land-use*. International Network for Bamboo and Rattan (INBAR) and Delft University of Technology, Faculty of Industrial Design Engineering, Design for Sustainability Program, Beijing, People's Republic of China.

Varela S, Correal JF, Yamin L and Ramírez F (2013) Cyclic performance of glued laminated Guadua bamboo-sheathed shear walls. *Journal of Structural Engineering* **139(11)**: 2028–2037.

Verma CS and Chariar VM (2012) Development of layered laminate bamboo composite and their mechanical properties. *Composites Part B: Engineering* **43(3)**: 1063–1069.

Villegas M (2003) *New Bamboo: Architecture and Design*. Villegas editores, Bogotá, DC, Colombia.

Vogtländer J, van der Lugt P and Brezet H (2010) The sustainability of bamboo products for local and Western European applications. LCAs and land-use. *Journal of Cleaner Production* **18(13)**: 1260–1269.

Xiao Y, Inoue M and Paudel SK (2008) Modern bamboo structures. In *Proceedings of the 1st International Conference on Modern Bamboo Structures (ICBS 2007)* (Xiao Y, Inoue M and Paudel SK (eds)). Taylor & Francis Group, London, UK, pp. 5–21.